Strength of radial breathing mode in single-walled carbon nanotubes

M. Machón,[1] S. Reich,[2] H. Telg,[1] J. Maultzsch,[1] P. Ordejón,[3] and C. Thomsen[1]

[1]*Institut für Festkörperphysik, Technische Universität Berlin, Hardenbergstrasse 36, 10623 Berlin, Germany*

[2]*Department of Engineering, University of Cambridge, Trumpington Street, Cambridge CB2 1PZ, United Kingdom*

[3]*Institut de Ciència de Materials de Barcelona, Campus de la Universitat Autònoma de Barcelona, 08193 Bellaterra, Barcelona, Spain*

(Received 2 August 2004; published 20 January 2005)

We show by *ab initio* calculations that the electron-phonon coupling matrix element $\mathcal{M}_{e\text{-}ph}$ of the radial breathing mode in single-walled carbon nanotubes depends strongly on tube chirality. For nanotubes of the same diameter the coupling strength $|\mathcal{M}_{e\text{-}ph}|^2$ is up to one order of magnitude stronger for zigzag tubes than for armchair tubes. For (n_1, n_2) tubes $\mathcal{M}_{e\text{-}ph}$ depends on the value of $(n_1 - n_2)$ mod 3, which allows us to discriminate semiconducting nanotubes with similar diameter by their Raman scattering intensity. We show measured resonance Raman profiles of the radial breathing mode which support our theoretical predictions.

The radial breathing mode (RBM) is without doubt the best known feature in the Raman spectra of carbon nanotubes. In this vibration all carbon atoms move in the radial direction creating a breathinglike deformation of the entire tube. This mode is unique to single-walled carbon nanotubes and is taken as indicative of the presence of nanotubes in a sample. Moreover, the frequency of the radial breathing mode is proportional to the inverse diameter of the tube.[1] Raman scattering is therefore often used to determine the diameter or diameter distribution in nanotube samples.[2–4] In detail, the relation between nanotube diameters in real samples and the radial breathing mode spectrum is more complicated, because of the resonances in the Raman process and additional force constants coming from the tube-tube van der Waals interaction in bundled nanotubes.[3,5,6] Furthermore, the RBM eigenvector has a small nonradial component.[7,8]

It was suggested to use the RBM to find not only the tube diameter but also the chiral angle, i.e., to identify a particular (n_1, n_2) nanotube.[4,9,10] n_1 and n_2 specify the chiral vector **c** $= n_1 \mathbf{a}_1 + n_2 \mathbf{a}_2$ around the circumference of a nanotube in terms of the graphene unit cell vectors $\mathbf{a}_1$ and $\mathbf{a}_2$. This assignment relied mostly on the frequency of the RBM, sometimes combined with an argument about the resonant enhancement of the Raman intensity for the laser excitation energy.[4] It was, however, always assumed that the electron-phonon coupling of the RBM is independent of the chirality of a tube.[11] This means that far from resonance or exactly in resonance the scattering intensity of the radial breathing mode is expected to be the same for different (n_1, n_2) nanotubes. Only recently a smaller matrix element for armchair tubes than for zigzag tubes was suspected from measurements of the RBM signal strength of a series of carbon nanotubes in solution.[12,13]

In this paper we show that, contrary to the widespread assumption, the electron-phonon coupling strength of the radial breathing mode depends on the diameter *and* chirality of the nanotube. In *ab initio* calculations we find the squared electron-phonon matrix elements in zigzag tubes to be up to one order of magnitude stronger than in armchair tubes for the same optical transition energy. In semiconducting nano-

tubes the matrix elements allow us to distinguish between the $(n_1 - n_2)$ mod $3 = \pm 1$ nanotube families. A similar intensity difference is expected for the two transitions of metallic nanotubes in each branch of the Kataura plot.[14] We show experimental evidence of this intensity difference based on measurements of resonant Raman profiles of the RBM of nanotubes in aqueous solution. The relative Raman intensities can independently confirm an (n_1, n_2) assignment obtained, e.g., by photoluminescence.

In the expression for the Raman-scattering cross section from perturbation theory the square of the electron-phonon matrix elements $|\mathcal{M}_{e\text{-}ph}|^2$ appears in the numerator. The intensity of the Raman signal in full resonance is scaled by the electron-phonon coupling.[15] When calculating these matrix elements both electrons and holes must be taken into account. To every electron excited into a conduction band c and interacting with a phonon corresponds a hole in the valence band v. Adding up the two contributions, i.e., assuming strict electron-hole symmetry, we obtain for the electron-phonon matrix element

$$\mathcal{M}_{e\text{-}ph} = \langle \mathbf{k}c | H_{e\text{-}ph} | \mathbf{k}c \rangle - \langle \mathbf{k}v | H_{e\text{-}ph} | \mathbf{k}v \rangle, \qquad (1)$$

where the minus sign comes from the opposite charges of holes and electrons.

The diagonal matrix elements of the electron-phonon coupling Hamiltonian $H_{e\text{-}ph}$ for optical phonons can be obtained from the shift of the electronic bands under deformation of the atomic structure corresponding to the phonon-pattern[16]

$$\langle \mathbf{k}, b | H^i_{e\text{-}ph} | \mathbf{k}, b \rangle = \sqrt{\frac{\hbar}{2MN\omega^i_{\text{RBM}}}} \sum_a \epsilon^i_a \frac{\partial E_b(\mathbf{k})}{\partial \mathbf{u}_a}, \qquad (2)$$

where the sum runs over all atoms in the unit cell. **k** and b denote, respectively, the wave vector and band index of the electronic state, i indexes the phonon, M is the atomic mass, ϵ^i_a is the polarization vector of the phonon, normalized as $\Sigma_a \epsilon^i_a \epsilon^j_a = \delta_{ij}$, $E_b(\mathbf{k})$ is the electronic energy and $\mathbf{u}_a$ is the atomic displacement. N is the number of unit cells in the system (1 in our calculation).

We calculated the Γ-point phonon spectrum and the band structure of several isolated nanotubes in their minimum-
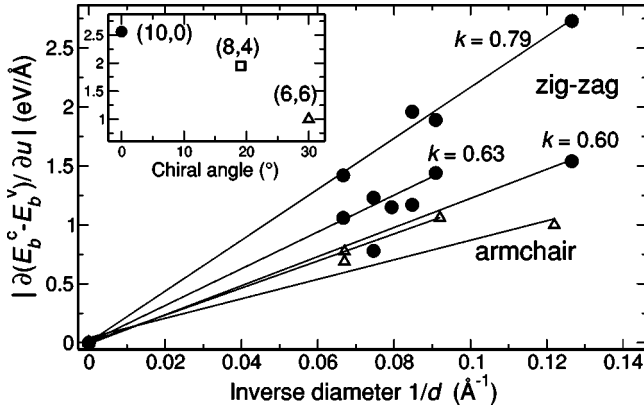
FIG. 1. Calculated band-energy changes (absolute value) per unit change in radius for zigzag (circles) and armchair tubes (triangles). Lines are linear fits of the data corresponding to the indicated k value [as defined in the horizontal axis of Fig. 2(c)]; they include the origin as a data point. Inset: Band-energy change $|\partial E_b(\mathbf{k})/\partial \mathbf{u}|$ for the first optical transition of nanotubes with diameter ≈ 8 Å as a function of the chiral angle.

energy configuration and under deformation due to the RBM to obtain the change of the electronic energies in Eq. (2).[17] The RBM eigenvector was obtained from finite differences; it has a small nonradial component[7,8] which lowers the calculated matrix elements by $\approx 30\%$. All calculations were performed with the SIESTA code[18] within the local density approximation.[19] The core electrons were replaced by nonlocal norm-conserving pseudopotentials.[20] A double-ζ, singly polarized basis set of localized atomic orbitals was used for the valence electrons, with cutoff radii of 5.12 a.u. for the s and 6.25 a.u. for the p and d orbitals.[21] Sixteen k points in the k_z direction were included for metallic nanotubes and three k points for semiconducting tubes. Real-space integrations were done in a grid with a cutoff ≈ 270 Ry.

In Fig. 1 we show the energy change $\partial E_b(\mathbf{k})/\partial \mathbf{u}$

$= \partial [E_b^c(\mathbf{k}) - E_b^v(\mathbf{k})]/\partial \mathbf{u}$ for several tubes as a function of inverse tube diameter. The data were evaluated at the region of the Brillouin zone with the highest optical transition probability, i.e., the band extrema.[22] We grouped the data corresponding to k points that are close when mapped onto the graphene Brillouin zone (lines in Fig. 1). To first approximation, the points of a particular group correspond to the same transition energies. We find that for a particular transition energy, $|\partial E_b(\mathbf{k})/\partial \mathbf{u}|$ is proportional to $1/d$ and tends to zero in the infinite-diameter limit. This trend can be easily understood, since the same change in radius yields smaller bond-length changes for bigger tube radii. The infinite-diameter limit corresponds to a translation of graphene, which cannot affect the electronic system. It is clearly seen that $|\partial E_b(\mathbf{k})/\partial \mathbf{u}|$ for zigzag tubes is up to 2.5 times larger than for armchair tubes. The inset of Fig. 1 shows the energy change for the first transition of tubes all with diameter ≈ 8 Å but different chiralities; in particular, the (8,4) tube lies between the armchair and the zigzag values. The assumption of a chirality-independent electron-phonon interaction is thus incorrect. Our results suggest the use of relative Raman *intensities* for discriminating chiralities.

In Table I, the calculated matrix elements and RBM frequencies are summarized; we found $\omega_{\mathrm{RBM}} \approx C_1/d + C_2$ with $C_1 = 232$ cm^{-1} nm in excellent agreement with the literature[23,24] and $C_2 = -6$ cm^{-1}. The largest difference in the matrix elements $\mathcal{M}_{e\text{-}ph}$ between zigzag (boldface) and armchair nanotubes of similar diameter and, hence, the same RBM frequency, is found for the (11,11) and the (19,0) tubes. The matrix element $\mathcal{M}_3$ of the (19,0) tube is by a factor of 3 larger than $\mathcal{M}_1$ of the (11,11) tube although the two transition energies are similar (see Table I). Since the Raman signal is proportional to $|\mathcal{M}_{e\text{-}ph}|^2$, we expect the RBM intensity to be nine times larger for the (19,0) than for the (11,11) nanotube from the difference in $|\mathcal{M}_{e\text{-}ph}|$ alone. For different transition energies this ratio could be even larger.

The matrix elements of zigzag tubes show another inter-

TABLE I. Calculated diameters, RBM frequencies, and electron-phonon matrix elements $\mathcal{M}_{e\text{-}ph}$ (in eV) for the first optical transitions (*ab initio* calculated energies in eV in parentheses[22]). The matrix elements (boldface for zigzag tubes) were rounded to 0.001 eV. Rows labeled $\mathcal{M}_{1-4}$ correspond to the first four optical transitions for light polarized parallel to the nanotube axis. A "—" indicates a lack of the transition or a band shift which could not be evaluated for technical reasons. Note that $\mathcal{M}_{e\text{-}ph}$ is normalized to the unit-cell volume V_c.

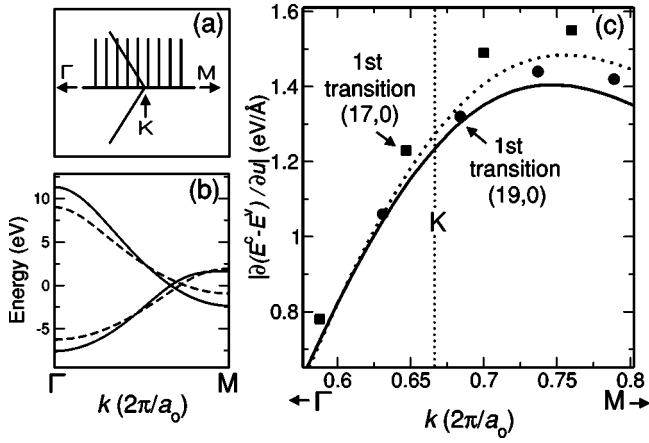|	(6,0)	(10,0)	(6,6)	(8,4)	(11,0)	(8,8)	(14,0)	(15,0)	(16,0)	(17,0)	(11,11)	(19,0)
V_c(Å^3)	77.2	210	130	626	254	230	406	467	534	603	436	755
d(Å)	4.8	7.9	8.2	8.4	8.7	10.9	11.0	11.8	12.6	13.4	15.0	15.0
ω_{ph}(cm^{-1})	446	287	278	274	257	209	203	188	179	170	151	149
$\mathcal{M}_1$	**0.050**	**−0.028**	−0.015	−0.013	**0.021**	−0.010	**0.016**	**−0.022**	**−0.017**	**0.014**	−0.005	**−0.015**
	(1.0)	(0.8)	(2.3)	(0.8)	**(0.9)**	(1.8)	(0.7)	(1.5)	(0.6)	(0.6)	(1.4)	(0.5)
$\mathcal{M}_2$	**−0.062**	**0.017**	—	0.004	**−0.028**	−0.015	**−0.020**	**0.013**	**0.013**	**−0.016**	−0.010	**0.012**
	(1.7)	(2.0)		(1.7)	**(1.3)**	(3.1)	(1.1)	(2.0)	(1.2)	(1.0)	(2.5)	(1.0)
$\mathcal{M}_3$	—	**−0.030**	—	−0.016	**−0.028**	−0.017	**−0.021**	**−0.022**	**−0.018**	**−0.017**	−0.012	**−0.016**
		(2.4)		(2.6)	**(2.6)**	(3.7)	(2.4)	(2.6)	(1.9)	(2.1)	(3.3)	(1.6)
$\mathcal{M}_4$	—	**−0.031**	—	—	**−0.028**	—	—	**−0.022**	—	**0.009**	—	**−0.016**
		(3.0)			**(3.1)**			(3.2)		(2.4)		(2.7)

FIG. 2. (a) Detail of the Brillouin zone (BZ) of graphene around K with the band lines of a (19,0) nanotube and the Γ-KM line. (b) Electronic bands of graphene along Γ-K-M in equilibrium (solid line) and under a deformation of 0.1 Å corresponding to the RBM of a (19,0) tube (dashed line, difference enhanced $\times 10$). (c) Calculated $\partial E_b(\mathbf{k})/\partial \mathbf{u}$ for a (17,0) (squares) and a (19,0) (circles) tube, and of graphene deformed to simulate the RBM of a (19,0) tube (solid line) and a (17,0) nanotube (dotted line).

esting feature: they have either a larger magnitude and are negative or a smaller magnitude and are positive [e.g., for the (10,0) tube $\mathcal{M}_1 = -0.028$ and $\mathcal{M}_2 = +0.017$. A change in sign is very uncommon in electron-phonon interaction in solid-state systems. The matrix elements are positive in most semiconductors.[25] To explain this unusual behavior we calculated $\partial E_b^{c,v}(\mathbf{k})/\partial \mathbf{u}$ of a graphene sheet ($a_0^{\text{equil.}} = 2.467$ Å) stretching the sheet in the zigzag direction to simulate the radial atomic displacement and adding the nonradial component (see Fig 2).

In Fig. 2(c) we show $|\partial E_b(\mathbf{k})/\partial \mathbf{u}|$ for graphene when stretching it according to a (19,0) tube (solid line) and a (17,0) tube (dotted line) together with the *ab initio* calculated values for these two tubes. The sign and magnitude of $\mathcal{M}_{e\text{-}ph}$ depend on where the optical transition occurs with respect to the K point of graphene. The Γ-point states of an $(n,0)$ zigzag tube in the graphene BZ are obtained by dividing the Γ-K-M line into n parts [see Fig. 2(a)]. The states closest to the K point of graphene have the lowest transition energies. The (17,0) tube, e.g., has its first transition to the left of the K point and the second one to the right. The energy shift of the graphene bands is smaller to the left of the K-point than to its right [Fig. 2(c)]. Therefore for this tube $|\mathcal{M}_1/\mathcal{M}_2| < 1$. The (19,0) tube, on the other hand, has its first transition to the right of the K point and the second to the left, yielding $|\mathcal{M}_1/\mathcal{M}_2| > 1$. Furthermore, $\partial E_b(\mathbf{k})/\partial \mathbf{u}$ is negative to the right of the K point, and positive to the left, explaining the signs of $\mathcal{M}_{e\text{-}ph}$. In general, all semiconducting tubes can be divided into $\nu = (n_1 - n_2) \bmod 3 = \pm 1$ families, which behave like the (17,0) and (19,0) tube with respect to sign and relative magnitude of the $\mathcal{M}_{e\text{-}ph}$. Metallic nanotubes usually have two close-by transition energies due to trigonal warping.[26] The transition with lower energy originates from the right of the K point, the one with higher energy from its left. Therefore, the lower-energy transition is expected to give a higher Raman intensity.
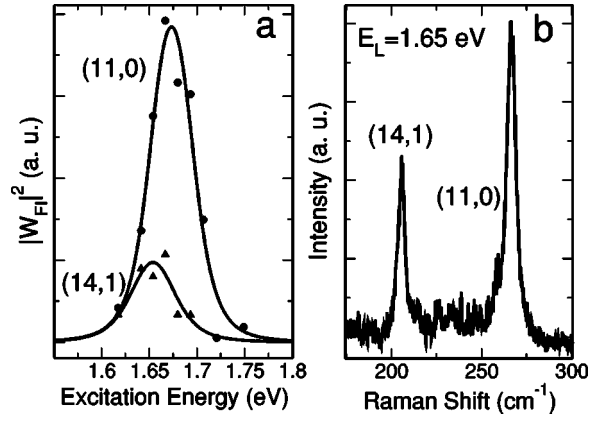

FIG. 3. (a) Measured resonance Raman profiles (symbols) and fits (lines) of two different nanotubes. (b) Raman spectrum with a laser energy of 1.65 eV.

To confirm our theoretical predictions we performed Raman scattering measurements on nanotubes in solution.[27,28] Raman spectra were excited with a Ti-sapphire laser, recorded with a DILOR XY800 spectrometer, and corrected for the sensitivity of the experimental setup. We then calculated the squared scattering amplitudes $|W_{FI}|^2$ from the Raman signal.

In Fig. 3(a) we show two selected resonance profiles of radial breathing modes. Using the assignment by Bachilo *et al.*[27] we identify these resonances as the second transition of the (14,1) nanotube with $\nu = +1$ and the (11,0) tube with $\nu = -1$.[29] We predicted a higher Raman intensity for nanotubes with $\nu = -1$ in excellent agreement with the experimental data. As shown in Fig. 1 $\partial E_b(\mathbf{k})/\partial \mathbf{u}$ is similar for nanotubes with similar diameter, chiral angle, and ν. Approximating the matrix element for the (14,1) tube by $\partial E_b(\mathbf{k})/\partial \mathbf{u}$ for the (16,0) nanotube we find theoretically $|\mathcal{M}_2^{(11,0)}/\mathcal{M}_2^{(14,1)}|^2 \approx 3$. Experimentally, the ratio $|W_{FI}^{(11,0)}/W_{FI}^{(14,1)}|^2 \approx 4$ is in excellent agreement with our *ab initio* result and a uniform distribution of chiral angles in nanotube samples.[30] We stress that the intensity difference between $\nu = -1$ and $+1$ tubes is generally observed in our experiment and not limited to the two profiles shown. A more detailed study is underway, but is beyond the scope of this paper.

Raman-based (n_1, n_2) assignments performed so far relied strongly on a Raman intensity analysis[4] that implicitly assumed constant electron-phonon coupling. As shown, this is not correct. The most intense peak does not necessarily correspond to the nanotube closest to resonance. As an example, we show in Fig. 3(b) a Raman spectrum for an excitation energy of 1.65 eV. This excitation energy corresponds to the maximum in the resonance profile of the (14,1) nanotube, whereas the (11,0) nanotube is excited 25 meV below its resonance. The Raman intensity thus depends not only on the resonance condition, but also on the particular tubes under study. Differences in Raman intensity due to resonances cannot be distinguished from the chiral angle dependence of $\mathcal{M}_{e\text{-}ph}$ using only a single excitation energy; instead a resonance profile has to be evaluated.

A chirality-dependent electron-phonon coupling naturally explains the observations by Strano *et al.*[12] They mapped the

electronic transitions of metallic nanotubes using Raman excitation profiles. Strangely, the armchair tubes were apparently missing in their sample. In contrast, photoluminescence experiments on the same type of sample[27] suggested a predominance of large-chiral-angle tubes. Our calculations solve this apparent contradiction: the Raman signal of armchair nanotubes is small due to a weak electron-phonon coupling.

In conclusion, we calculated the electron-phonon matrix elements for carbon nanotubes. The matrix elements of zigzag tubes are much larger than those of armchair tubes, leading to a larger Raman signal for smaller chiral angle tubes. Furthermore, for semiconducting tubes the magnitude and the sign of the matrix elements change systematically for different optical transitions and $\nu=\pm 1$ nanotubes. Relative Raman intensities can discriminate between armchair and zigzag tubes as well as $\nu=\pm 1$ tube families. The latter we demonstrated by measuring the radial breathing mode resonance on a -1 and $+1$ nanotube. The family and chiral-angle dependence of the Raman intensities can be used for a refined assignment of chiral indices and chirality distributions.

[1] A. M. Rao, E. Richter, S. Bandow, B. Chase, P. C. Eklund, K. A. Williams, S. Fang, K. R. Subbaswamy, M. Menon, A. Thess, R. E. Smalley, G. Dresselhaus, and M. S. Dresselhaus, Science **275**, 187 (1997).
[2] S. Bandow, S. Asaka, Y. Saito, A. M. Rao, L. Grigorian, E. Richter, and P. C. Eklund, Phys. Rev. Lett. **80**, 3779 (1998).
[3] M. Milnera, J. Kürti, M. Hulman, and H. Kuzmany, Phys. Rev. Lett. **84**, 1324 (2000).
[4] A. Jorio, R. Saito, J. H. Hafner, C. M. Lieber, M. Hunter, T. McClure, G. Dresselhaus, and M. S. Dresselhaus, Phys. Rev. Lett. **86**, 1118 (2001).
[5] U. D. Venkateswaran, A. M. Rao, E. Richter, M. Menon, A. Rinzler, R. E. Smalley, and P. C. Eklund, Phys. Rev. B **59**, 10 928 (1999).
[6] C. Thomsen, S. Reich, A. R. Goñi, H. Jantoljak, P. Rafailov, I. Loa, K. Syassen, C. Journet, and P. Bernier, Phys. Status Solidi B **215**, 435 (1999).
[7] E. Dobardžić, I. Milošević, B. Nikolić, T. Vuković, and M. Damnjanović, Phys. Rev. B **68**, 045408 (2003).
[8] J. Kürti, V. Zólyomi, M. Kertesz, and G. Sun, New J. Phys. **5**, 125 (2003).
[9] C. Kramberger, R. Pfeiffer, H. Kuzmany, V. Zólyomi, and J. Kürti, Phys. Rev. B **68**, 235404 (2003).
[10] R. R. Bacsa, A. Peigney, C. Laurent, P. Puech, and W. S. Bacsa, Phys. Rev. B **65**, 161404(R) (2002).
[11] E. Richter and K. R. Subbaswamy, Phys. Rev. Lett. **79**, 2738 (1997).
[12] M. S. Strano, S. K. Doorn, E. H. Haroz, C. Kittrell, R. H. Hauge, and R. E. Smalley, Nano Lett. **3**, 1091 (2003).
[13] S. K. Doorn, D. A. Heller, P. W. Barone, M. L. Usrey, and M. S. Strano, Appl. Phys. A: Mater. Sci. Process. **78**, 1147 (2004).
[14] H. Kataura, Y. Kumazawa, I. Umezu, S. Suzuki, Y. Ohtsuka, and Y. Achiba, Synth. Met. **103**, 2555 (1999).
[15] C. Trallero-Giner, A. Cantarero, M. Cardona, and M. Mora, Phys. Rev. B **45**, 6601 (1992).
[16] F. Khan and P. Allen, Phys. Rev. B **29**, 3341 (1984).
[17] M. Verissimo-Alves, R. B. Capaz, B. Koiller, E. Artacho, and H. Chacham, Phys. Rev. Lett. **86**, 3372 (2001).
[18] J. M. Soler, E. Artacho, J. D. Gale, A. García, J. Junquera, P. Ordejón, and D. Sánchez-Portal, J. Phys.: Condens. Matter **14**, 2745 (2002).
[19] J. P. Perdew and A. Zunger, Phys. Rev. B **23**, 5048 (1981).
[20] N. Troullier and J. Martins, Phys. Rev. B **43**, 1993 (1991).
[21] J. Junquera, O. Paz, D. Sánchez-Portal, and E. Artacho, Phys. Rev. B **64**, 235111 (2001).
[22] S. Reich, C. Thomsen, and P. Ordejón, Phys. Rev. B **65**, 155411 (2002).
[23] J. Kürti, G. Kresse, and H. Kuzmany, Phys. Rev. B **58**, R8869 (1998).
[24] D. Sánchez-Portal, E. Artacho, J. M. Soler, A. Rubio, and P. Ordejón, Phys. Rev. B **59**, 12 678 (1999).
[25] M. Cardona, in *Light Scattering in Solids II*, edited by M. Cardona and G. Güntherodt, Topics in Applied Physics Vol. 50 (Springer, Berlin, 1982), p. 19.
[26] S. Reich and C. Thomsen, Phys. Rev. B **62**, 4273 (2000).
[27] S. M. Bachilo, M. S. Strano, C. Kittrel, R. H. Hauge, R. E. Smalley, and R. B. Weisman, Science **298**, 2361 (2002).
[28] H. Telg, J. Maultzsch, S. Reich, F. Hennrich, and C. Thomsen, Phys. Rev. Lett. **93**, 117401 (2004); H. Telg, J. Maultzsch, S. Reich, F. Hennrich, and C. Thomsen, in *Structural and Electronic Properties of Synthetic Nanostructures*, edited by H. Kuzmany, J. Fink, M. Mehring, and S. Roth (Melville, New York, 2004), AIP Conf. Proc. **723**, 330 (2004).
[29] Bachilo *et al.*[27] provide an empirical formula which reproduces their measurements in a systematic manner and allows an assignment of our peaks. It yields $E_{22}=1.676$ eV and $\omega_{RBM}=207$ cm^{-1} for the (14,1) nanotube, providing the best match with our peak at 206 cm^{-1}. For the second peak, both (11,0) and (10,2) nanotubes provide a good match. Our argumentation does not depend strongly on this particular assignment and we therefore assign this peak to the (11,0) nanotube, which can be directly compared with the theory. The (14,1) peak in Fig. 3(b) contains a resonant contribution from other nanotubes not shown in (a) for clarity.
[30] L. Henrard, A. Loiseau, C. Journet, and P. Bernier, Synth. Met. **103**, 2533 (1999).